

# **Analysis of the longitudinal space charge impedance of a round uniform beam inside parallel plates and rectangular chambers**

L. Wang

*SLAC National Accelerator Laboratory, Menlo Park, CA 94025, USA*

Y. Li

*Department of Physics, Michigan State University, East Lansing, MI 48824, USA*

(Dated: Jul 10, 2014)

This paper analyses the longitudinal space charge (LSC) impedances of a round uniform beam inside a rectangular and parallel plate chamber using image charge method. The analysis is valid for arbitrary wavelengths and the calculation converges fast. The research shows that only a few of image beams are needed to get a relative error less than 0.1%. The beam offset effect is also included in the analysis.

PACS numbers: 29.27.Bd, 29.20.db

## **I. INTRODUCTION**

The LSC impedances are important factors that should be taken into account in the design and operation of modern particle accelerators, especially the ones with low energy and high beam intensities which are prone to microwave instabilities induced by the LSC fields [1, 2]. It is even important for Free Electron Lasers (FELs) where the electron's energy is up to a few GeV but with very high peak current on the order of kA [3]. Strong micro-bunch on the order of micrometer have been recently observed [4] in Linac Coherent Light Source (LCLS) [5] at SLAC National Accelerator Lab (SLAC). Various LSC field models have been proposed and studied extensively by different methods in the existing literatures, such as Refs. [6-11]. In many accelerators, the configurations of the real beam and chamber system can be simplified as a field model consisting of a round beam moving inside a rectangular chamber. When the aspect ratio of the cross-section of the rectangular chamber is large, it can be simplified further as a pair of parallel plates [12]. If the beam has longitudinal density modulations, due to mismatch of the cross-sectional shapes between the beam and chamber, the exact closed-form solutions to the three-dimensional (3D) space charge fields and the corresponding LSC impedances of the above two cases cannot be obtained by the method of separation of variables. Though Ref. [6] used the method of conformal mapping and Faraday's law applying to a rectangular integral loop to derive the analytical expressions for the LSC fields and impedances of a round beam in rectangular chamber, it neglects the 3D field effects when the density perturbation wavelength is small. Hence this method and results are only valid in the long-wavelength limits and are not appropriate for the study of microwave or micro-bunching instabilities. Since in most accelerators, the ratios of the transverse chamber dimensions to the beam diameters are large, Ref. [11] provided the approximate solutions to the field models of a round beam with planar and rectangular boundary conditions, assuming the 3D image charge fields of the round beam can be approximated by those of a line charge, the resulting LSC fields and impedances are valid for the whole perturbation wavelength spectrum. When the ratio of the beam diameter to the transverse chamber dimension approaches unity, the relative errors of the calculated LSC impedances will become larger.

This paper proposes an image charge method to calculate the LSC impedances of a round beam between parallel plates and inside a rectangular chamber. Since the solutions to the LSC fields of a round uniform beam with sinusoidal line charge density modulations in free space are available in a closed form [5], if the beam were placed inside a rectangular chamber or between parallel plates, due to planar symmetry and mirroring, the associated total image charge fields of the infinite chain (parallel plates model) or grid (rectangular chamber model) of the image beams can be calculated by simple summation. Adding the self-fields of the round beam in free space, the total LSC fields and impedances of the two models in discussion can be obtained. Through case study, we found the calculated LSC fields and impedances converge fast with the number of image beams, usually only a finite, small number of image beams are needed to obtain the LSC fields and impedances with relative errors less than 0.1%. The resolution of the calculated LSC fields and impedances depend on the number of image charges used in the calculation, rather than the ratio of the beam diameter to the transverse chamber dimension as the case in Ref [11].

This paper is organized as follows. Section II briefly introduces the wave equations describing the space charge fields of the charged beam. Section III briefly introduces the numerical calculation method for general geometry of the beam and beam pipe. Section IV provides a short review for the LSC fields and impedances of a round beam in free space and inside a round chamber. Sections V and VI calculate the LSC impedances of a round beam between parallel plates and inside a rectangular chamber using the image charge method, respectively.

## II. WAVE EQUATIONS

The wave equation describing the electric field is

$$\nabla^2 \mathbf{E} - \frac{1}{c^2} \frac{\partial \mathbf{E}}{\partial t} = \frac{\nabla \rho}{\epsilon_0} + \mu_0 \frac{\partial \mathbf{J}}{\partial t} \quad (1)$$

where  $\rho$  and  $\mathbf{J}$  are the charge and the current densities, respectively. They obey the following continuity equation:

$$\frac{\partial \rho}{\partial t} + \vec{\nabla} \cdot \mathbf{J} = 0. \quad (2)$$

Assuming that the beam is moving with a constant longitudinal speed  $\mathbf{v} = \beta c \hat{\mathbf{z}}$  along the  $z$  axis, both the line charge density and beam current density have sinusoidal modulations with frequency  $\omega$  along the longitudinal coordinate  $z$ , we can represent its charge density  $\rho$ , current density  $\mathbf{J}$  and beam current  $I$  by the following relations:

$$\rho(x, y, z, t) = \lambda_z \rho_{\perp}(x, y) e^{-i\omega(t-z/v)}, \quad (3a)$$

$$\mathbf{J} = \rho \mathbf{v} = \hat{\mathbf{z}} \beta c \lambda_z \rho_{\perp}(x, y) e^{-i\omega(t-z/v)}, \quad (3b)$$

$$I = \lambda_z v e^{-i\omega(t-z/v)} = \bar{I} e^{-i\omega(t-z/v)}, \quad (3c)$$

where  $\lambda_z$  is the line charge density,  $\rho_{\perp}$  is the transverse beam distribution function,  $\beta$  is the relativistic speed of the beam,  $c$  is the speed of light. We will work with the  $z$ -components of the vectors  $\mathbf{E}$ ,  $\mathbf{J}$  and  $\nabla$ .

$$\frac{\partial J_z}{\partial t} = -i\omega v \lambda_z \rho_{\perp} e^{-i\omega\left(t-\frac{z}{v}\right)}, \quad (4)$$

$$\frac{1}{\varepsilon_0} \frac{\partial \rho}{\partial z} = \frac{i\omega \lambda_z}{\varepsilon_0 v} \rho_{\perp} e^{-i\omega\left(t-\frac{z}{v}\right)}. \quad (5)$$

The  $z$ -component of electric field can be written as

$$\mathbf{E}_z(x, y, z, t) = \hat{\mathbf{z}} E_z(x, y) e^{-i\omega\left(t-\frac{z}{v}\right)}. \quad (6)$$

Substituting Eqs. (4-6) into Eq. (1), the amplitude of longitudinal electric field satisfies the following equation

$$\left(\nabla_{\perp}^2 - \frac{k^2}{\gamma^2}\right) E_z = i \frac{k \lambda_z}{\varepsilon_0 \gamma^2} \rho_{\perp}(x, y), \quad (7)$$

where  $\nabla_{\perp}^2 = \frac{\partial^2}{\partial x^2} + \frac{\partial^2}{\partial y^2}$ ,  $k = \frac{\omega}{v} = \frac{\omega}{\beta c}$  and  $\frac{1}{\gamma^2} = 1 - \frac{v^2}{c^2} = 1 - \beta^2$ .

The longitudinal impedance is defined as

$$Z_{||}(k) = -\frac{1}{I} \int_0^{\infty} \mathbf{E}_z dz = -\frac{1}{\lambda_z \beta c} \int_0^{\infty} E_z dz. \quad (8)$$

### III. FEM SIMULATION FOR ARBITRARY GEOMETRY

Eq. (7) with arbitrary cross-sectional geometries of the beam and beam pipe can be solved numerically using Finite Element Method (FEM) method. The FEM equation is

$$\left(\mathbf{M} + \frac{k^2}{\gamma^2} \mathbf{B}\right) \mathbf{E} = \mathbf{Q}, \quad (9)$$

with

$$M_{ij}^e = \iint_S \left( \frac{\partial N_i}{\partial x} \frac{\partial N_j}{\partial x} + \frac{\partial N_i}{\partial y} \frac{\partial N_j}{\partial y} \right) dx dy, \quad (10)$$

$$B_{ij}^e = \iint_S N_i N_j dx dy, \quad (11)$$

$$Q_i^e = -i \frac{k q_i}{\varepsilon_0 \gamma^2}. \quad (12)$$

where  $q_i$  is the charge at the node  $i$ , which is proportional to the harmonic charge density  $\lambda_z$ . The current  $I$  has the similar dependence on  $\lambda_z$ . Therefore, the LSC impedance given by Eq.(8) is independent of the line charge density as expected.

### IV. IN FREE SPACE AND INSIDE A ROUND CHAMBER

For an infinitely long round beam with uniform transverse density within radius  $a$ , its transverse density distribution is

$$\rho_{\perp}(r) = \begin{cases} \frac{1}{\pi a^2} & (r \leq a) \\ 0 & (r > a) \end{cases}, \quad (13)$$

where  $r^2 = x^2 + y^2$ . The general solution of Eq. (7) with the above beam distribution is

$$E_z(r) = \begin{cases} A_1 I_0\left(\frac{kr}{\gamma}\right) + A_2 K_0\left(\frac{kr}{\gamma}\right) & r > a, \\ A_3 I_0\left(\frac{kr}{\gamma}\right) - i \frac{\lambda_z}{k \pi a^2 \varepsilon_0} & r \leq a. \end{cases} \quad (14)$$

where  $I_0(x)$  and  $K_0(x)$  are the 0<sup>th</sup> order modified Bessel functions of the first and second kinds, respectively. In free space, the field strength at infinitely far distance is finite. Therefore  $A_1=0$ . The continuity conditions of the field and its derivative at  $r=a$  give [5]

$$E_z^{free}(r) = \begin{cases} -i \frac{\lambda_z}{k\pi a^2 \varepsilon_0} \left[ 1 - \frac{ka}{\gamma} K_1\left(\frac{ka}{\gamma}\right) I_0\left(\frac{kr}{\gamma}\right) \right] & (r \leq a), \\ -i \frac{\lambda_z}{k\pi a^2 \varepsilon_0} \left[ \frac{ka}{\gamma} K_0\left(\frac{kr}{\gamma}\right) I_1\left(\frac{ka}{\gamma}\right) \right] & (r > a). \end{cases} \quad (15)$$

where  $I_1(x)$  and  $K_1(x)$  are the 1<sup>st</sup> order modified Bessel functions of the first and second kinds, respectively. The superscript “free” on the left hand stands for “free space”. With the property of  $I_0(0)=1$ , Eqs. (8)(15) give the LSC field and impedance per unit length on the beam axis ( $r=0$ ) as

$$E_z^{free}(0) = -i \frac{\lambda_z}{k\pi a^2 \varepsilon_0} \left[ 1 - \frac{ka}{\gamma} K_1\left(\frac{ka}{\gamma}\right) \right], \quad (16)$$

$$\frac{Z_{||}^{free}(k)}{L} = i \frac{Z_0}{k\pi a^2 \beta} \left[ 1 - \frac{ka}{\gamma} K_1\left(\frac{ka}{\gamma}\right) \right]. \quad (17)$$

where  $Z_0 = 1/\varepsilon_0 c \approx 377 \text{ Ohms}$  is the impedance of free space. Since the longitudinal electric field depends on the radial position, the LSC impedance also has the same dependence. The LSC impedance per unit length for arbitrary  $r$  with  $r < a$  (within the beam) is given by

$$\frac{Z_{||}^{free}(k,r)}{L} = i \frac{Z_0}{k\pi a^2 \beta} \left[ 1 - \frac{ka}{\gamma} K_1\left(\frac{ka}{\gamma}\right) I_0\left(\frac{kr}{\gamma}\right) \right]. \quad (18)$$

Inside a round beam chamber, the continuity conditions at  $r=a$  and the boundary condition on the chamber surface  $E_z(r=r_w)=0$  determines the coefficients  $A_1$ ,  $A_2$  and  $A_3$  in Eq. (14), thus the final solution of the longitudinal electric field is

$$E_z^{rd}(r) = \begin{cases} -i \frac{\lambda_z}{k\pi a^2 \varepsilon_0} \left\{ 1 - \frac{ka}{\gamma} \frac{I_0\left(\frac{kr}{\gamma}\right)}{I_0\left(\frac{kr_w}{\gamma}\right)} \left[ K_1\left(\frac{ka}{\gamma}\right) I_0\left(\frac{kr_w}{\gamma}\right) + K_0\left(\frac{kr_w}{\gamma}\right) I_1\left(\frac{ka}{\gamma}\right) \right] \right\}, & (r \leq a) \\ -i \frac{\lambda_z}{k\pi a^2 \varepsilon_0} \frac{ka}{\gamma} I_1\left(\frac{ka}{\gamma}\right) \left[ K_0\left(\frac{kr}{\gamma}\right) - \frac{K_0\left(\frac{kr_w}{\gamma}\right)}{I_0\left(\frac{kr_w}{\gamma}\right)} I_0\left(\frac{kr}{\gamma}\right) \right]. & (a < r \leq r_w) \end{cases} \quad (19)$$

The superscript “rd” on the left hand side stands for “round chamber”. The above equation gives the well-known LSC impedance per unit length of a round uniform beam inside a round beam chamber [13]

$$\frac{Z_{||}^{rd}(k,r)}{L} = i \frac{Z_0}{k\pi a^2 \beta} \left\{ 1 - \frac{ka}{\gamma} \frac{I_0\left(\frac{kr}{\gamma}\right)}{I_0\left(\frac{kr_w}{\gamma}\right)} \left[ K_1\left(\frac{ka}{\gamma}\right) I_0\left(\frac{kr_w}{\gamma}\right) + K_0\left(\frac{kr_w}{\gamma}\right) I_1\left(\frac{ka}{\gamma}\right) \right] \right\}. \quad (20)$$

## V. BETWEEN PARALLEL PLATES

We apply the image method in a stepwise fashion by disregarding the boundary at each plate. Fig. 1 shows the image charges of a source point between a pair of parallel plates where the red and blue dots represent the positive and negative charges, respectively. All the image charges have the same charge amount as the source charge. The distances of the source point to the upper and lower plates are  $d$  and  $g$ , respectively. The full separation between the two plates is  $h=g+d$ . If the source charge is located on the median plane between the two plates, then we have  $g=d=h/2$ .



where  $R_n = \sqrt{x^2 + (y_i(n) - y)^2}$ . The superscript “*pp*” on the left hand of Eq. (21) stands for “*parallel plates*”. The first and second terms on the right hand side of Eq. (21) are contributed from the original source beam and the image beams, respectively. Using Eqs. (8)(15) and (21), we obtain the LSC impedance at position  $(x, y)$  inside the beam as

$$\frac{Z_{||}^{pp}(k,x,y)}{L} = i \frac{Z_0}{k\pi a^2 \beta} \left[ 1 - \frac{ka}{\gamma} K_1\left(\frac{ka}{\gamma}\right) I_0\left(\frac{kR_0}{\gamma}\right) + \frac{ka}{\gamma} I_1\left(\frac{ka}{\gamma}\right) \sum_{|n|=1}^{\infty} (-1)^{|n|} K_0\left(\frac{kR_n}{\gamma}\right) \right]. \quad (22)$$

Different from the free space case, the LSC field of a round beam between parallel plates is not axisymmetric around the beam axis due to the boundary shape. Therefore, the impedance is a function of  $(x, y)$ , instead of solely  $r$ .

Fig. 3 shows an example of the calculated *on-axis* impedance with different number of image beams. The full height of the parallel plate is  $h=4a$  in this example. The image charges affect the impedance mostly in the long-wavelength regime where  $\gamma/(ka) > 1$ . This clearly explains why the shielding is effective only for long wavelength. The impedance with  $|n|=1$  has the smallest value because it includes only the first image beam which has opposite charge sign with respect to the original beam. On the other hand, the impedance with  $|n|=2$  has the maximum value. Similarly,  $|n|=3$  gives the second smallest one and  $|n|=4$  gives the second largest one and so on. When  $|n|$  is large enough the variation of the impedance is negligible, because the image beams are far away from the source beam and the field finally converges.

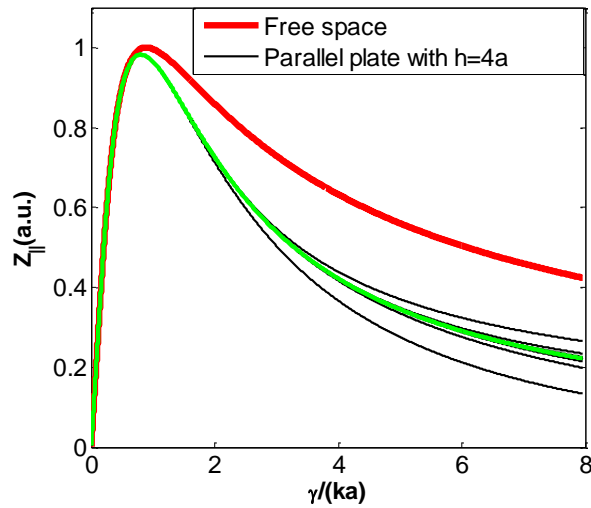


FIG.3. The effects of image bunches on the *on-axis* LSC impedance of a round uniform beam between parallel plate chamber. The bunch has a radius of  $a=5$  mm and the full height of the parallel plate is  $h=4a=20$  mm. The family of black lines shows the calculated impedances with different number of image charge  $n$  in Eq. (22) from 1 to 20. The green line in the plot shows the calculated impedance with  $|n|=20$ .

Fig. 4 shows the variation of the *on-axis* LSC impedance at  $\gamma/(ka) = 8$  with the number of image beams. The calculated impedance (blue curve) oscillates with the number of image beams at small  $n$  and converges to one value at large  $|n|$ . The relative error (red curve) in the plot is the absolute value of the

relative error. The true errors oscillate with  $|n|$  and have negative errors with odd number of  $|n|$ . The absolute relative errors decay exponentially with  $|n|$  which implies that the field converges quickly. An image beam number  $|n|=15$  gives a relative error in the order of magnitude of  $10^{-4}$ .

When the beam axis has vertical offsets with respect to the chamber median plane, the *on-axis* LSC impedance at long wavelength is slightly reduced as shown in Fig. 5 assuming  $h=10a$  and the beam offsets range from  $1\sim 4a$ . The beam offset affects only the long wavelength impedance for the same mechanism as the shielding effect. When the beam axis shifts vertically from the chamber median plane, one group of images moves closer to the beam while another group of images moves away from it as shown in Fig. 1. The net effect from the re-distribution of the image beams is small due to the cancellations of all the image beams. In general case, the effect of beam offset is negligible if the offset amplitude is small compared with the aperture of beam pipe.

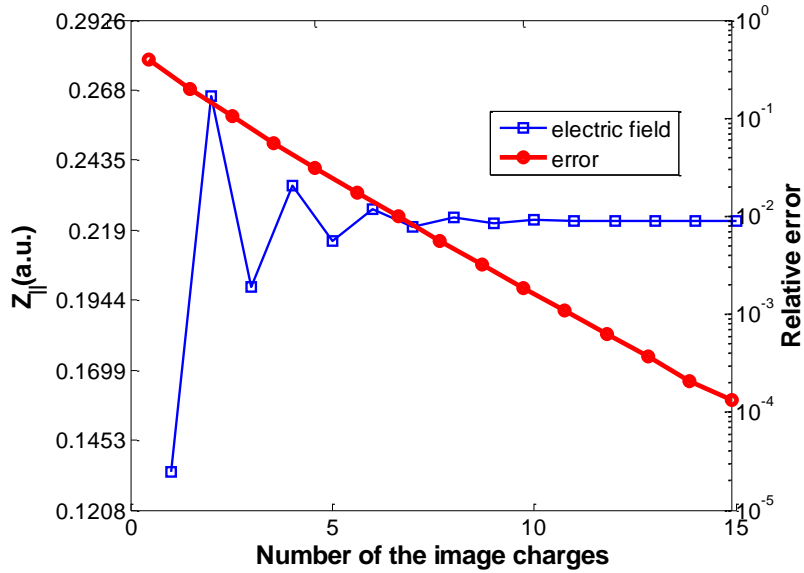


FIG. 4. Convergence of the *on-axis* LSC impedance with the number of image charge. This result corresponds to the case  $\gamma/ka = 8$  as shown in FIG. 3 where the image charge effect is relatively larger.

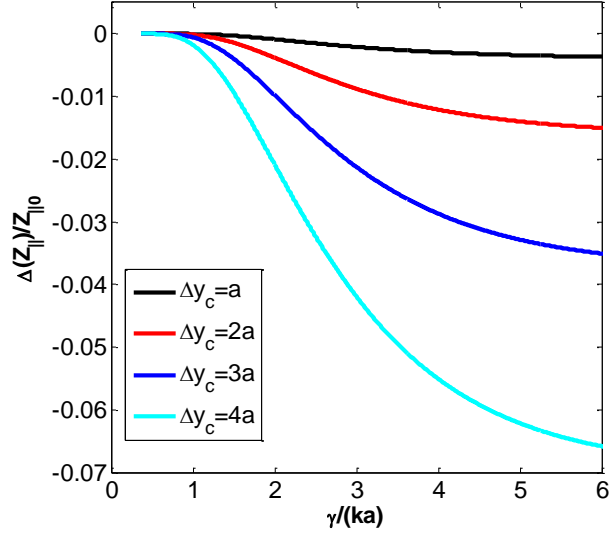


FIG. 5. Effect of vertical beam axis offset ( $\Delta y_c$ ) on the *on-axis* LSC impedance of a parallel plate chamber with  $h=10a$ . The relative impedance difference is normalized by the *on-axis* LSC impedance with  $\Delta y_c=0$ . The impedance at long wavelength is slightly reduced when the beam axis has small vertical offsets.

## VI. INSIDE A RECTANGULAR CHAMBER

Consider a rectangular conducting structure with full width  $w$  and full height  $h$ . We assume the axes of the rectangular chamber and the beam are located at  $(0, 0)$  and  $(x_c, y_c)$ , respectively. Fig. 6 shows the image points of a point charge inside a rectangular chamber. The red and blue dots represent the positive and negative charges, respectively.

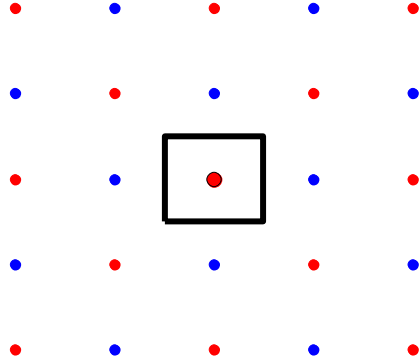


FIG. 6. 2D grid of images of a point charge inside a rectangular chamber.

Through planar symmetry and mirroring, we can determine the exact coordinates of images of a point charge inside a rectangular chamber with alternating positive and negative images as

$$x_i(m, n) = mw + (-1)^{|m|}x_c,$$

$$y_i(m, n) = nh + (-1)^{|n|}y_c,$$

$$\lambda(m, n) = \lambda_z(-1)^{|m|+|n|}, m = n = 0, \pm 1, 2, 3 \dots \quad (23)$$

Here  $m$  and  $n$  represent the indexes of the image grid points in horizontal and vertical directions, respectively. For instance,  $m > 0$  ( $m < 0$ ) are the images with  $x > 0$  ( $x < 0$ ). The image with the indexes of  $m = n = 0$  is just the original point charge. Similar to the parallel plate case, the image beams of a round uniform beam still keep the round uniform distributions with the same beam radius as the source beam, while the centers of the image beams are given by Eq. (23). Therefore, the LSC fields at  $(x, y)$  within the beam inside a rectangular chamber is the total LSC fields of the original beam and its image beams

$$E_z^{rect}(x, y) = \sum_{m=-\infty}^{\infty} \sum_{n=-\infty}^{\infty} (-1)^{|m|+|n|} E_z^{free}(R_{m,n}), \quad (24)$$

with  $R_{m,n} = \sqrt{(x_i(m, n) - x)^2 + (y_i(m, n) - y)^2}$ . The superscript “*rect*” on the left hand of the equation stands for “*rectangular chamber*”. Note that the original charge effect is included with  $m = n = 0$ . Using Eqs. (8) (15) (24), we obtain the LSC impedance per unit length at position  $(x, y)$  inside the beam as

$$\frac{Z_{||}^{rect}(k, x, y)}{L} = i \frac{Z_0}{k\pi a^2 \beta} \left[ 1 - \frac{ka}{\gamma} K_1\left(\frac{ka}{\gamma}\right) I_0\left(\frac{kR_{0,0}}{\gamma}\right) + \frac{ka}{\gamma} I_1\left(\frac{ka}{\gamma}\right) \sum_{\substack{m=-\infty \\ m \neq 0}}^{\infty} \sum_{\substack{n=-\infty \\ n \neq 0}}^{\infty} (-1)^{|m|+|n|} K_0\left(\frac{kR_{m,n}}{\gamma}\right) \right]. \quad (25)$$

FIG. 7 shows the comparisons of the *on-axis* LSC impedances between the theoretical calculations and the simulation results using a Finite Element Method (FEM) code. We used the 20 keV ( $\beta \approx 0.0046$ ,  $\gamma \approx 1.0$ ) coasting  $H_2^+$  beam in Small Isochronous Ring (SIR) at Michigan State University (MSU) [12] in this example. The chamber of SIR is rectangular with  $w=11.4$  cm and  $h=4.8$  cm. The number of images used in the calculation is 10. The *on-axis* LSC impedances of the beam with four different beam radii are compared to each other. The analytical results (solid lines) and FEM results (circles) perfectly overlap each other demonstrating excellent agreements in all cases.

The *on-axis* LSC impedance of a round uniform beam inside a rectangular chamber in the long wavelength limit is [6]

$$\frac{Z_{||}^{rect, LW}(k)}{L} = i \frac{Z_0 k}{2\pi\beta\gamma^2} \left[ \frac{1}{2} + \ln\left(\frac{2h}{\pi a} \tanh\left(\frac{\pi w}{2h}\right)\right) \right]. \quad (25)$$

This equation largely overestimates the impedance at short wavelength as shown by the dashed lines in Fig. 7. Therefore, it is essential to use a more accurate LSC impedance formula working at any wavelength in the study of beam instability. From the above equation, we can obtain the *on-axis* LSC impedance in the limiting case of  $w \rightarrow \infty$  (parallel plate) as [14]

$$\frac{Z_{||}^{pp, LW}(k)}{L} = i \frac{Z_0 k}{2\pi\beta\gamma^2} \left[ \frac{1}{2} + \ln\left(\frac{2h}{\pi a}\right) \right]. \quad (26)$$

Similar to the rectangular chamber case, Eq. (26) only works well in the long-wavelength limit.

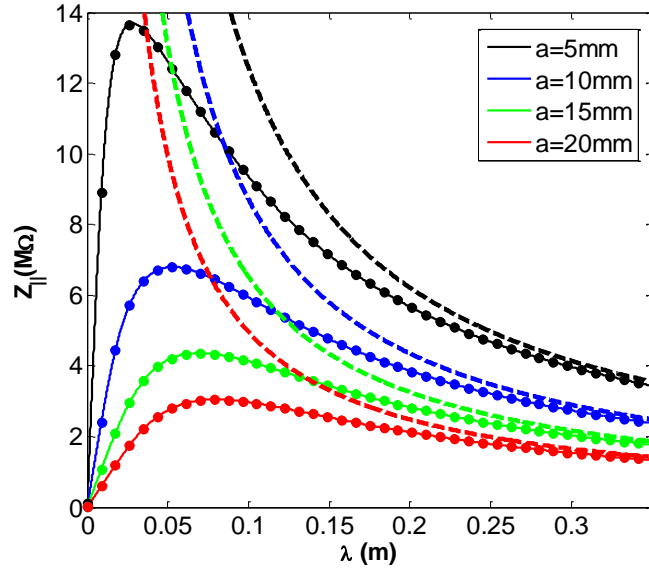


FIG.7. Comparisons of the *on-axis* LSC impedance of round uniform beam inside a rectangular chamber between analysis (solid lines) and FEM (solid dots). The long-wavelength limit results (dashed lines) are also shown for comparisons. The parameters used in the calculations are  $w = 11.4 \text{ cm}$ ,  $h = 4.8 \text{ cm}$ , the variable beam radii are  $a = 0.5, 1.0, 1.5$  and  $2.0 \text{ cm}$  in this study. The circumference of SIR is  $6.58 \text{ m}$ .

Fig. 8 shows the shielding effects of a squared chamber with  $w=h=4a, 6a, 8a, \dots, 16a$ . The shielding effect is negligible at short wavelengths with  $\gamma/ka < 1.0$ , while it becomes effective at long wavelengths. For a fixed beam radius, the shielding effect becomes weaker as the chamber aperture is large because the image beams are farther away from the source beam.

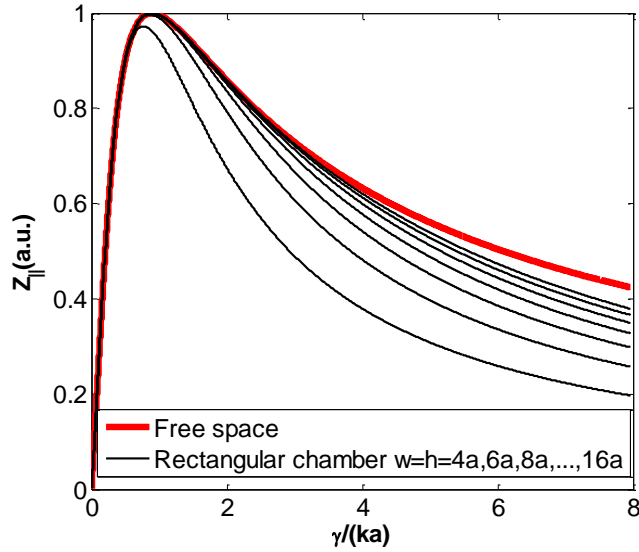


FIG. 8. The shielding effect of a rectangular chamber. The round uniform beam has a radius of  $a$ , the full widths and heights of the chamber are  $w=h=4a, 6a, 8a, 10a, 12a, 14a$  and  $16a$ , which correspond to the lower to upper black lines as clearly shown on the right part of the plot.

Fig. 9 compares the shielding effect between a round chamber and a rectangular chamber as a function of the aspect ratios  $w/h$  of the rectangular chamber. The round chamber has slightly stronger shielding than a squared chamber resulting in a smaller *on-axis* LSC impedance, which is about 6% (1%) less than that of round beam inside a square pipe when the pipe radius is  $2a$  ( $10a$ ) at long-wavelength regime with  $\gamma/ka > 2$ . When the aspect ratio of rectangular chamber is larger than 2, the shielding effect is very close to that of a parallel plate model.

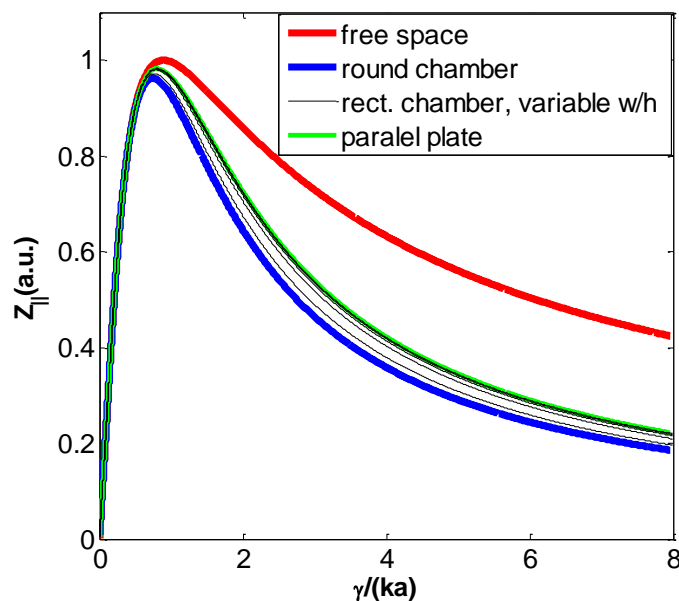


FIG. 9. Comparisons of the shielding effects between a round chamber and a rectangular chamber as a function of the ratio  $w/h$ , where  $w/h=1, 1.25, 1.5, 1.75, 2$ . The height of the rectangular chamber  $h$  is fixed and equal to the diameter of the round chamber.

All the impedances shown in the figures so far are evaluated on the beam axis with  $x=y=r=0$  in Eq. (22) and Eq. (25). Our analyses also give the impedances averaged over the beam cross-section. Fig. 10 shows the *average* LSC impedance of the round beam with four different boundary conditions: parallel plates, squared chamber, round chamber, and in free space, respectively. The same beam parameters and normalization are used as in Fig. 9, where the normalized peak impedance in free space is set to 1. The shielding effects on the *average* LSC impedances are similar to the case of *on-axis* LSC impedances. The *average* LSC impedance of the round beam is about 20% less than the *on-axis* one when  $1 < \gamma/(ka) < 8.0$ . However, they are almost identical for high frequency with  $\gamma/(ka) < 1.0$ .

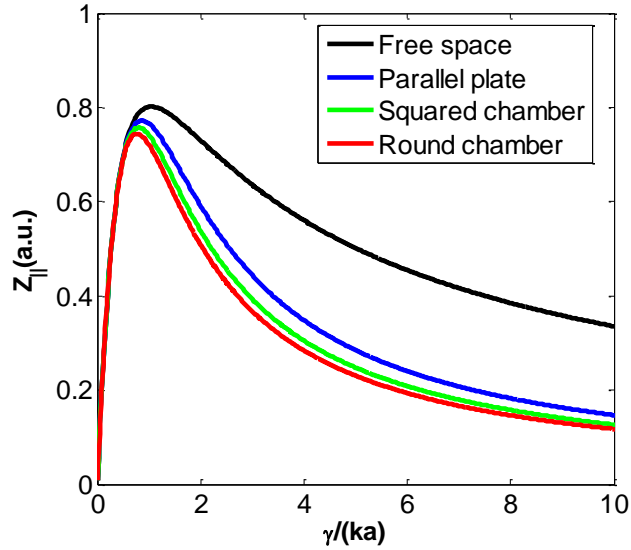


FIG. 10. Comparisons of the shielding effects between round, squared, and parallel plate chambers on the *average* LSC impedance. The same beam and chamber parameters are used as in FIG. 9

## VII. CONCLUSIONS

The image charge method is employed in this paper to provide analytical solutions to the LSC impedances of a round uniform beam with line charge modulations inside a rectangular chamber and between parallel plates, respectively. Though the solutions consist of contributions from an infinite number of image beams, due to the fast convergence with the number of image beams, only a finite and small number of image beams are needed to get satisfying resolutions. Since the solutions to the image charge fields induced by each constituent image beam are exact and expressed in a closed form, the resolutions of the total calculated LSC fields and impedances are only dependent on the number of image beams used in the calculation, and insensitive to the ratios of transverse dimensions between the chamber and beam. This is a general method applicable to other beam distributions, such as Gaussian, rectangular and elliptic beams. The calculated LSC impedances in our analyses are valid in the full wavelength spectrum and at arbitrary position within the beam. Moreover, the effects of beam axis offset are also included in our analysis.

Our studies show that round chambers have slightly better shielding effect than squared chambers. When the aspect ratio of a rectangular chamber is larger than 2, the shielding effect is very close to that of a pair of parallel plates. The effect of beam axis offset in general is small if the beam is not extremely close to the chamber.

## ACKNOWLEDGEMENTS

Author Wang would like to thank Prof. Zhirong Huang at SLAC for fruitful discussions.

## REFERENCES

---

- [1] E. Pozdeyev, J. A. Rodriguez, F. Marti, R.C. York, Phys. Rev. ST Accel. Beams **5** 054202 (2009).
- [2] Y. Li, L. Wang, Nucl. Instrum. Methods Phys. Res., Sect. A, in press, DOI: 10.1016/j.nima.2014.06.070 (2014).
- [3] Z. Huang, M. Borland, P. Emma, J. Wu, C. Limborg, G. Stupakov and J. Welch, Phys. Rev. ST Accel. Beams **7**, 074401 (2004).
- [4] D. Ratner, private communications
- [5] P. Emma, et al., Nat. Photon. **4**, 641 (2010).
- [6] K. Y. Ng, Part. Accel. **16** (1984) 63.
- [7] J. Rosenzweig, C. Pellegrini, L. Serafini, C. Ternienden and G. Travish, TESLA FEL-Report 1996-15.
- [8] S. Humphries, Jr., *Charged Particle Beams*, Wiley, New York, 1990, p. 704.
- [9] R. D. Ryne, <http://arxiv.org/abs/1111.4971>.
- [10] Y. Li, L. Wang, Nucl. Instrum. Methods Phys. Res., Sect. A **747** (2014) 30–36.
- [11] Y. Li, L. Wang, <http://arxiv.org/abs/1403.6468>.
- [12] E. Pozdeyev, Ph.D thesis, Michigan State University (2003).
- [13] J. L. Laclare, CERN Accelerator School, CERN 85-19, p. 381.
- [14] C. E. Nelson and A. M. Sessler, Review of Scientific Instruments, **30**(02), 1959, 80-89.